ACS APPLIED MATERIALS & INTERFACES

Research Article

www.acsami.org

Enhancing the Tunability of the Open-Circuit Voltage of Hybrid Photovoltaics with Mixed Molecular Monolayers

Lee Barnea-Nehoshtan,[†,§] Pabitra K. Nayak,[†,§] Andrew Shu,[‡] Tatyana Bendikov,[⊥] Antoine Kahn,[‡] and David Cahen*[,†]

[†]Department of Materials and Interfaces and [⊥]Department of Chemical Research Support, Weizmann Institute of Science, Rehovot 76100, Israel

[‡]Department of Electrical Engineering, Princeton University, Princeton, New Jersey, 08544, United States

Supporting Information

ABSTRACT: The alignment between the energy levels of the constituents of an organic solar cell plays a central role in determining the open-circuit voltage. However, tuning the energy levels of electrodes and/or active components via molecular modifiers placed at interfaces is not straightforward. The morphology of organic materials is commonly controlled by the substrate onto which they are deposited, and differences in morphology often lead to differences in energetics. Such a change in morphology may reduce the effect of surface modifications, as the modified surface is part of an interface with the organic material. Here we show, in an experimental model system, that by using binary molecular monolayers, in which dipolar molecules are buried in a protective nonpolar matrix, we can transform changes in the electrode surface dipole into interface dipole changes without significantly affecting the growth of pentacene onto the molecular layer, thus enabling the use of the full range of dipolar-induced open-circuit-voltage tuning.

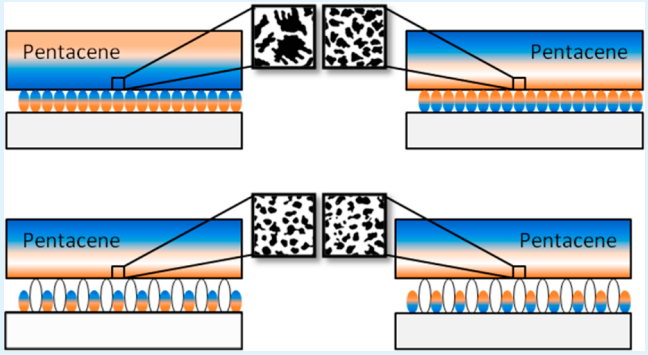

KEYWORDS: *organic photovoltaics, mixed monolayers, Energy alignment, Interface dipole, pentacene, UV photoemission spectroscopy*

INTRODUCTION

Organic semiconducting materials (OSC) are attractive for use in optoelectronic devices like solar cells, as these materials are potentially low cost, readily available, and can be made by simple processing. Also, the fabrication techniques for OSC-based devices are relatively straightforward, making such cells also attractive in terms of "green compliance". As the exciton binding energy in OSCs can be hundreds of meV,[1] solid-state OSC-based solar cells often combine organic absorbers with other organic or inorganic semiconductors to separate the photogenerated excitons into quasi-free charge carriers. Often it is the organic/organic or organic/inorganic interface that plays a pivotal role in the solar cell performance, and particularly in the open-circuit voltage (V_{oc}). In organic photovoltaic cells, whether polymer/fullerene bulk heterojunctions or planar heterojunctions, V_{oc} depends on a variety of factors that influence charge recombination. In particular, V_{oc} depends on the energetics of the charge-transfer states, formed between the electron donor (D) and electron acceptor (A) materials,[2−5] which primarily depends on the energy difference between the highest occupied molecular orbital (HOMO) of the electron-donor and the lowest unoccupied molecular orbital (LUMO) of the electron-acceptor. Therefore, increasing the V_{oc} requires proper matching of electronic levels of the materials involved,[6−13] quantities that can be measured either directly via photoemission, or deduced from other measurements. Nearly three decades of progress in organic photovoltaic cells have produced a variety of electron donor materials. However, the choice of electron transporting materials, whether organic materials as electron acceptors, or metal-oxides like TiO_2 and ZnO as electron collectors, remains comparatively limited. Therefore, the optimal energy alignment is sometimes compromised in favor of other considerations such as morphology and processability.

A dipole layer at the interface between donor and acceptor can shift the local vacuum level,[14] and impose a relative shift between the HOMO (D) and the LUMO (A), which can relax the requirements for the selection of D−A couples to optimize the V_{oc},[15−17] thus broadening the range of usable materials. Tada et al.[13] showed that tailor-made D and A molecules can be used at interfaces to control the V_{oc} of a cell. A noticeable drawback of this approach is that the presence of an interlayer affects not only the energy alignment, but also the morphology of the organic materials.[18−21] The morphology, in turn, determines bulk properties that are relevant for photovoltaic activity, such as absorbance, charge mobility,[18] and even the

Received: September 27, 2013
Accepted: January 27, 2014
Published: January 27, 2014

   dx.doi.org/10.1021/am4056134 | ACS Appl. Mater. Interfaces 2014, 6, 2317−2324

ionization potential of the material.[22−24] Many groups used surface modifications of substrate and contact materials, such as indium tin oxide[25] and ZnO,[26] to control the morphology of bulk heterojunction cells and, thus, the solar cell parameters. For solar cells with planar configuration of active materials, pentacene is one of the most widely used electron donors. Pentacene was extensively studied in terms of the effect of its morphology on the performance of organic solar cells[27,28] and organic field effect transistors.[29] As the organic film growth on (semi)conducting surfaces can give rise to change in energetics of the surface, it is important to know the evolution of the energetics on a surface that is already modified. Knowledge regarding the microscopic origin of the change can help to prepare better monolayers, to harness the maximum possible effect from dipolar molecular monolayers. Controlling the energetics at the active interface while maintaining or inducing the desired morphology can be a key factor in OSC-based optoelectronic device performance.

In this work, we show the use of silane-based binary molecular monolayers (MMs) as a pathway to decoupling the interface energetics and the morphology of the constituent phases. Silane-based MMs form a 2D network on the surface,[30,31] requiring much less binding sites per unit surface area than carboxylate-, phosphonate-, or thiol-based MMs, which require at least one binding site per molecule. Therefore, silanes can provide a route for modifying surfaces with low density of binding sites because of nonuniformity, or multiple crystallographic facets. The MMS are composed of short molecules with positive or negative polar head groups, embedded in a protective matrix of longer molecules with fixed weak dipole (alkyl chains, in our case). Using a model system with pentacene as electron donor and crystalline SIC as acceptor, we show how a binary monolayer at the active D/A interface enables the tuning of the energetics of a pentacene/SiC junction, while minimizing morphological effects on the pentacene layer, grown onto the MMs that contain different dipolar molecules.

Table 1. Summary of the Surface Work Function of the Functionalized SiC before and after Depositing Pentacene of Nominal Thickness of 2 nm[a] and the Open Circuit Voltages of the Devices Built with the Respective Monolayers

	Φ (eV) binary MM	Φ (eV) binary MM + pentacene	V_{oc} [mV] binary MM	Φ (eV) unary MM	Φ (eV) Unary MM + pentacene	V_{oc} (mV) unary MM
OTMS \HTMS	4.0	3.8	420	4.0	3.8	400
APTMS	3.7	3.5	500	3.7	3.7	430
FPTMS	4.3	4.1	310	4.4	4.1	300
range	0.6	0.6	190	0.7	0.4	70

[a]The values are averaged over 3 to 7 sets of UPS and CPD measurements. All work function values are given with ±0.1 eV certainty level, and all V_{oc} values with certainty level better than 10 mV.

EXPERIMENTAL SECTION

Sample Preparation. The ⟨0001⟩ surface of n-type 6H-SiC single crystal substrate were hydroxylated by repeated cycles of O_2 plasma oxidation and etching with hydrofluoric acid.[32]

The SiC was functionalized with self-assembled monolayers of propyl-silanes with either of two polar head groups: 3,3,3-(trifluoro-propyl)trimethoxy-silane (FPTMS) was used to induce a negative dipole and amino-propyl-trimethoxy-silane (APTMS) to induce a positive dipole.[33]

The conditions and duration of the incubation of the samples were optimized to obtain monolayers of a single component, i.e., unary MM samples. For binary MMs, the incubation was stopped at shorter times, when an average thickness of ∼70% of that of a monolayer was reached, as measured by ellipsometer (see below), before the APTMS or FPTMS molecules reach full coverage. Next, the sample was immersed in a solution of octyl-trimethoxy-silane (OTMS) solution, to fill the unoccupied sites. Further details on sample preparation are given in the Supporting Information (SI). MMs of hexyl-trimethoxy-silane (HTMS) and full-coverage OTMS were used as references.

Following MM deposition, the samples were heated to 80 °C under vacuum of $<4 \times 10^{-6}$ Torr. To follow the evolution of the surface work function (Φ), pentacene was deposited at a rate of 0.1−0.5 Å/s to a final thickness of 2 nm for photoemission measurements or 5 nm for Kelvin probe measurements (see description below). On several points along the

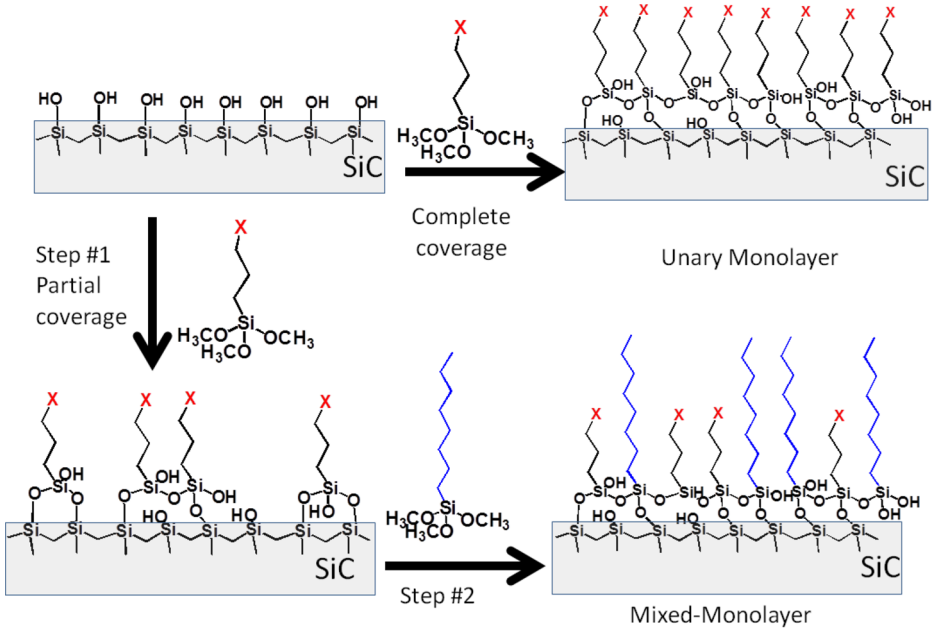

Figure 1. Schematic representation of grafting of different type of monolayers. In the case of mixed monolayers, the dipole-forming molecules (with X as headgroup) are masked by the longer alkyl chains.

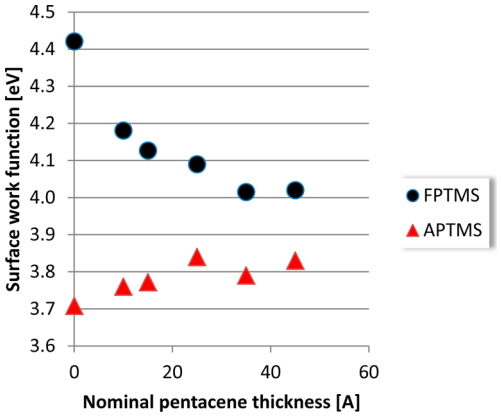

Figure 2. Work function of pentacene grown on SiC functionalized with unary FPTMS and APTMS MMs as the film becomes thicker. The work function was measured using a Kelvin probe under inert atmosphere. Above 20 Å, the change in work function is insignificant, within instrumental error.

deposition process, the samples were moved from the evaporation chamber to a measurement chamber under vacuum or inert atmosphere.

For device fabrication, a layer of 70 nm of pentacene was evaporated at a rate of 1−3 Å/s. A thin, 10 nm, film of gold was evaporated onto the pentacene through a shadow mask, to form a semitransparent top contact. The transparency of the evaporated contacts was over 80% across the visible spectrum.

Sample Characterization. The surface hydrophobicity was measured using the static water contact angle technique (SWCA). The surface hydrophobicity provides a rough estimation of the monolayer surface coverage, as the hydroxylated SiC is highly hydrophilic, with SWCA < 15°. The coverage of the monolayers was further verified by deducing their (optical) thickness from ellipsometry data, obtained with a spectroscopic ellipsometer (Woollam), and comparing the obtained values to the results from theoretical calculations, assuming all-trans configurations for the molecules.

The packing of the OTMS component in the binary and unary MMs was assessed with the help of Fourier-Transform IR spectroscopy in the attenuated total reflection mode, with a Germanium crystal, using the frequency of the CH_2 stretching mode. Because the <1700 cm^{-1} region is obscured due to the phonon mode of SiC, the presence of the functional head groups in the MMs was confirmed using X-ray photoemission spectroscopy.

To verify the homogeneity of the mixed monolayer, we scanned the monolayer-covered surface using an atomic force microscope (AFM) in the dynamic mode, and a Kelvin probe force microscope (KPFM) in an amplitude-modulated dual frequency mode.

The surface work function and the pentacene HOMO edge were measured using UV photoemission spectroscopy (UPS). Relative work function values were additionally obtained from contact potential differences (CPD), measured by macroscopic Kelvin probe in inert atmosphere.

The current−voltage characteristics of the solar cells were measured using a halogen light source, which was passed through a 530 nm long-pass filter to avoid any absorption by the 3 eV band gap SiC. The final illumination intensity was 30 mW/cm^2.

RESULTS AND DISCUSSION

Energy Level Evolution & Morphology. The adsorption of an OTMS MM on SiC does not alter the work function of the semiconductor, found to be 4.0 eV on the initial, hydroxylated[32] surface. This implies that the Si−O−Si bond formation between SiC and the silane anchoring group chain does not change the surface dipole from the one corresponding to the OH-termination of the surface. However, the adsorption of a molecules with the same anchoring group and an electron-withdrawing

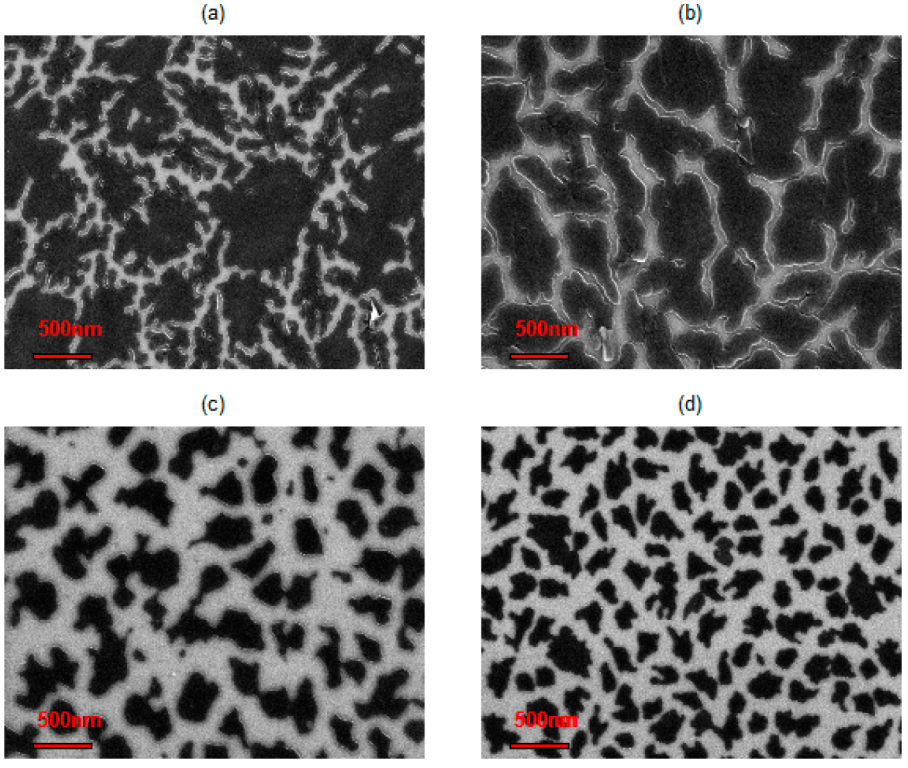

Figure 3. Scanning electron microscope micrographs of surfaces that are partially covered with pentacene on SiC, functionalized with MM of (a) unary APTMS, (b) binary APTMS, (c) unary FPTMS, and (d) binary FPTMS. The dark areas are the pentacene grains. The decrease in grain size is apparent in both types of MM, being more pronounced on the APTMS. The nominal pentacene thickness is 4 nm, which is an average measurement over a large area, containing patches with stacks of 1−3 molecules and empty (molecule-free) areas.

dx.doi.org/10.1021/am4056134 | ACS Appl. Mater. Interfaces 2014, 6, 2317−2324

($-CF_3$) or electron-donating ($-NH_2$) headgroup, replacing the ($-CH_3$) headgroup of the alkyl chain, does change the surface dipole with respect to the unmodified surface, as measured for the APTMS- and FPTMS-modified surfaces. This change is observed as a change in the CPD and a shift of the low-binding energy onset of the UPS signal. As seen in Table 1, the three unary (single component) MM-modified surfaces span a work function range of 0.7 eV. Deposition of pentacene on top of the MM further changes the surface work function. As seen in Figure 2, a sharp change occurs at pentacene thicknesses as small as 5 Å, suggesting the formation of a dipole. We observe an increase of Φ for the pentacene on APTMS-terminated surface, and a decrease of Φ for the pentacene FPTMS-terminated surfaces. Both the negative and positive interface dipoles are reduced with respect to the dipoles formed on the free surface. The work function continues to change as the first few monolayers are being deposited. After deposition of 20 Å of pentacene, no significant further change is observed, within the experimental errors of either the CPD or the UPS (cf. Figure S3 in the Supporting Information) measurements. Consequently, the effective work function range is reduced to 0.4 eV, for pentacene of 2 nm nominal thickness (cf. Table 1).

Moreover, the differences in the energy level alignments between the three MMs are accompanied by morphological differences in the deposited pentacene films. Scanning electron microscope micrographs show that the growth pattern of pentacene on the hydrophilic APTMS-covered surface (Figure 3a) with SWCA of 54 ± 1° is considerably different than the pattern of pentacene grown on the hydrophobic FPTMS-covered one (Figure 3c) with SWCA of 92 ± 1°. AFM topographical profiles further show the difference in the shape of the pentacene grains (nominal thickness 2 nm) formed on the two surfaces (Figure 4). The individual grains that

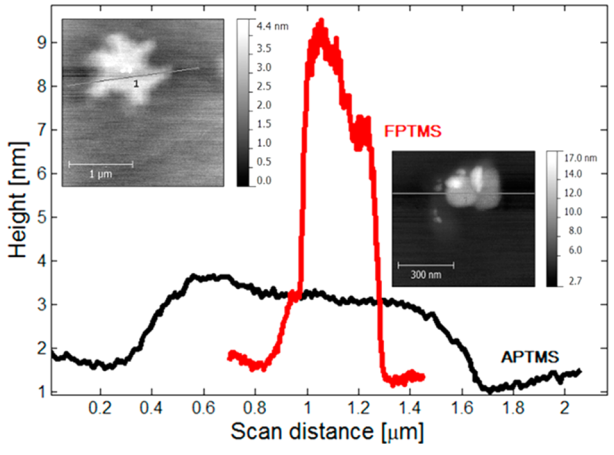

Figure 4. Individual grain of pentacene on SiC, functionalized with either an MM of unary APTMS or of FPTMS. The pentacene film was deposited simultaneously on both the samples.

were grown on the APTMS MM are higher and narrower than the ones on the FPTMS-covered surfaces. We note that a dendritic growth pattern of pentacene on a hydrophilic surface, such as the APTMS-functionalized SiC, was previously shown to result from dewetting if the sample was stored under vacuum[34] or if it was heated during or after deposition.[35] Our films are grown at a substrate temperature of 350 K and stored under vacuum for at least 30 min prior to further measurement or processing. Therefore, we can assume that the dewetting process is fully saturated, and that AFM, scanning electron microscope and device characterization were all conducted on samples of equal morphology. Hydrophobicity-dependent growth patterns of pentacene were also reported on MM-functionalized SiO_2,[18,19,36−38] as well as on other surfaces.[39]

The reduction in the range of interface dipole can be attributed to the change in the polarization of the pentacene, via its polarizability dependence on the grain size and stacking orientation. Such dependence of both magnitude and direction of polarizability was predicted by calculations[40,41] and demonstrated experimentally.[23,42,43]

To reduce the effect of the polar head groups on the growth morphology, we incorporate silanes with an octyl chain, to form a binary MM. Because these are longer than the dipolar molecules, the octyl chains separate the pentacene from the functional head groups of the shorter propyl silanes.

Upon switching to the binary MM, we obtain two MMs of similar hydrophobicity, with SWCA = 97 ± 1° for the FPTMS:OTMS mixture and 90 ± 1° for the APTMS:OTMS mixture. AFM and KPFM scans confirm that the binary mixture is homogeneous down to the 20 nm lateral resolution of these methods, i.e., no evidence for formation of segregated domains is obtained (see Figures S1 and S2 in the Supporting Information, and discussion therein). Figure 3b shows a film of pentacene grown on a binary APTMS MM. The pentacene grains lose most of their dendritic appearance, and become more similar in shape to the grains of pentacene grown on binary FPTMS MM (Figure 3d), as expected from the

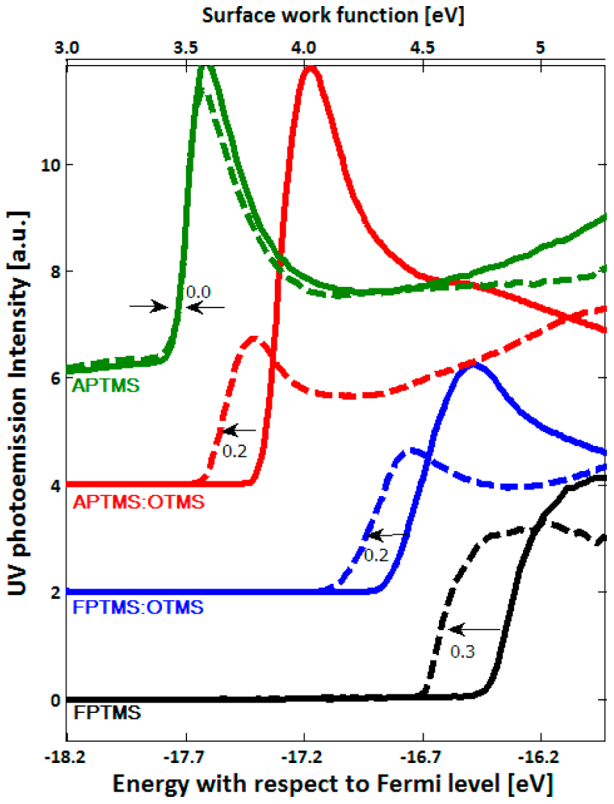

Figure 5. UPS He I spectra of SiC with unary and binary MM of APTMS and FPTMS before (solid lines) and after (dashed lines) being covered by a pentacene layer with nominal thickness of 2 nm. The secondary electron cutoff region is shown. The interface dipole formation is evident from the downward shift of the cut-off energy upon pentacene deposition on top of the hydrophobic MM, indicated by the arrows. The hydrophilic unary APTMS MM does not show an onset shift. The spectra were vertically shifted for clarity. Full spectra appear in Figure S5 in the Supporting Information.

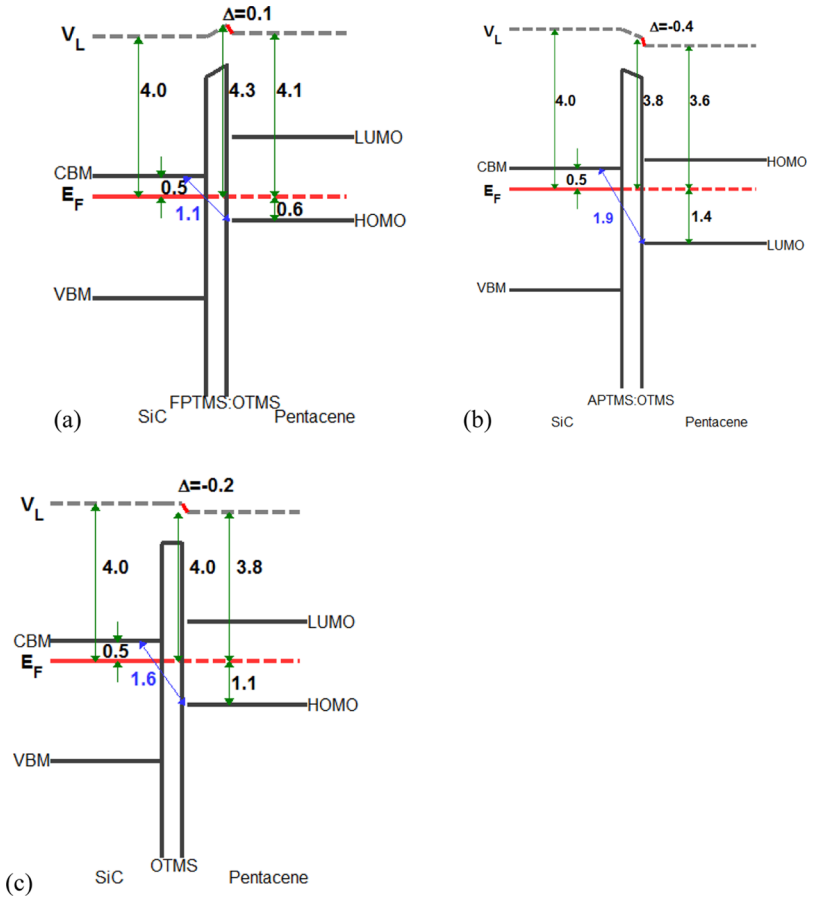

Figure 6. Energy diagrams for the junctions of SiC and pentacene with interlayer of (a) binary FPTMS MM, (b) binary APTMS MM, and (c) OTMS MM. On each diagram the surface work functions of the pristine SiC, and of the functionalized SiC before and after deposition of 2 nm of pentacene are indicated by green arrows. The local vacuum level (V_L), the Fermi level (E_F), the conduction band minimum (CBM), valence band maximum (VBM), HOMO and LUMO levels are also indicated. The red section of the V_L line demonstrates how the vacuum level shifts in the same direction (downward) for all three MMs.

increased similarity in hydrophobicity of the surfaces with both types of binary MMs. The dipoles that develop at the binary MM-modified SiC surface are lower than those at the unary MM -modified one (cf. Table 1). We attribute the decrease in dipole to the lower dipole concentration[44,45] of the polar propyl-silane component, and to the decay of the electric field over the distance between the functional headgroup and the outer surface of the binary MM, which is determined by the OTMS (cf. Figure 1). This is in contrast to previously reported results with binary MMs, where the reduction of surface dipole is due of the existence of two competing dipoles.[46] The work function range of the modified SiC surface is thus reduced slightly from 0.7 to 0.6 eV. Nevertheless, as shown in Figure 5 and Figure 6, the shifts in UPS onset for the pentacene films, deposited both on FPTMS- and on APTMS-based binary MMs, are not only in the same direction, but also of the same magnitude, contrary to the difference in magnitude of the shifts, found for pentacene on unary MM (cf. Table 1). No change is seen in the span of the dipole-induced Φ modulation of the free surface, when it is transformed into an interface with pentacene. The resulting range of 0.6 eV in Φ is thus 50% larger than the 0.4 eV observed for the samples built on unary MM. Most important, the work function span translates into a span of offsets between the pentacene HOMO and the bottom of the SiC conduction band. The resulting energy offsets are 1.6, 1.2, and 1.9 eV for OTMS-, FPTMS:OTMS-, and APTMS:OTMS-covered SiC, respectively.

Effect of Energetics and Morphology on Photovoltaic Cell. To illustrate the role of energetics at the interface, we fabricated solar cells with the above-discussed interfaces. To maintain the simplicity of our model system, we have not included any additional components such as hole-blocking or hole-transporting layers. The devices are thus nonoptimized and give low current densities.

Figure 7a shows the current−voltage characteristics for devices of pentacene grown on SiC functionalized with a binary or unary MM. The range of V_{oc} of devices with binary MM is larger than that with unary MM, as indicated by the scale bars. Additionally, the range of the J_{sc} is shown to decrease.

Figure 7b shows the change of the V_{oc} of the junctions with respect to the junction with an interlayer composed of nonpolar molecules only. The MMs introduce a dielectric spacer between the donor and acceptor material. As such, they may influence charge transfer and charge recombination rates. To negate a possible effect on the V_{oc} stemming from the difference in thickness between the binary and unary MM, we relate each sample to a reference sample of equal MM thickness. OTMS was used as a reference for binary MMs, and HTMS as a reference for the unary MMs. For both unary-MM and binary-MM based devices, the V_{oc} increases with decreasing surface work function. The modulation of the surface work function of the binary-MM functionalized surfaces is nearly 0.2 eV lower than that of the unary-MM functionalized surfaces. However,

dx.doi.org/10.1021/am4056134 | ACS Appl. Mater. Interfaces 2014, 6, 2317−2324

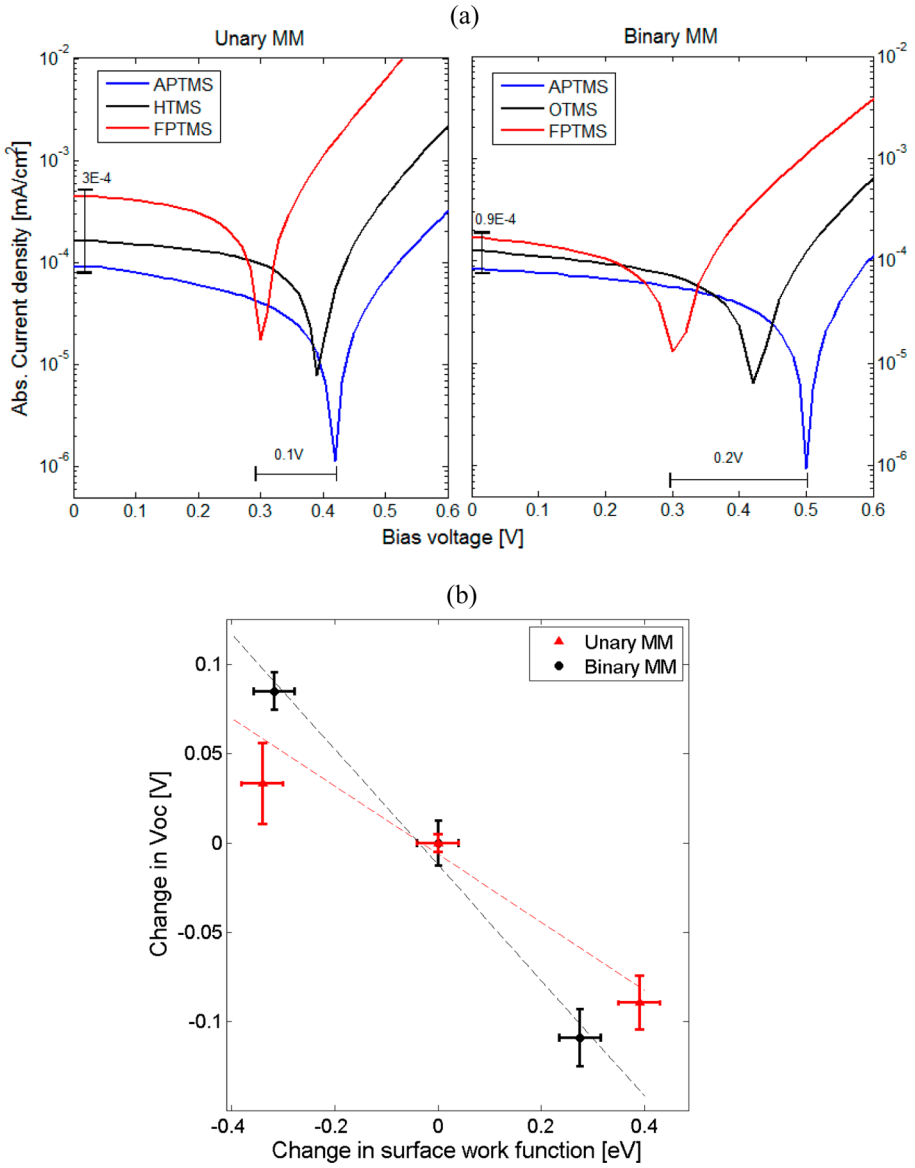

Figure 7. (a) Current−voltage characteristics of pentacene/MM/SiC device structures using unary and binary monolayers. Each curve is the average of 5−8 independent junctions on the same sample. The increase of Voc range and the decrease of J_{sc} range are indicated. (b) Change in the open-circuit voltage of pentacene/MM/SiC device structures upon changing the surface work function, using either a unary or binary monolayers. The error bars represent the range of V_{oc} results. The linear regressions (dotted lines) emphasize how the slope becomes steeper upon switching from unary to binary MM.

the modulation of the resulting V_{oc} in the binary-MM based devices is twice as large as that in the unary-MM based devices (cf. Table 1 and Figure 7). We can attribute the increased response to surface modification, to the increase in effective range of energy difference between the conduction band minimum of the SiC and the HOMO level of the pentacene.

CONCLUSIONS

We have shown how the use of mixed molecular monolayers that separate the dipole-determining molecular head groups from the organic absorber, can eliminate the unwanted and often uncontrolled effect of dipolar surface layers on the morphology of organic absorber film, grown on top of the MMs. We demonstrated that the use of binary molecular monolayers with buried dipoles minimizes this effect on the morphology of pentacene overlayers. Most importantly, the use of binary alkyl-silane monolayers with buried dipoles maintains the dipole of the free functionalized surface throughout the deposition of the organic overlayer, and enhances the tunability of the open circuit voltage of a hybrid organic\inorganic solar cell. Using the same molecules, the concept can be extended to other substrates that can be silanized, such as ZnO[47] or GaN[48] that are more relevant to applications in hybrid photovoltaics or hybrid field effect transistors. Further extensions with other binding groups, such as carboxylates and phosphonates on these and other semiconductors and contact materials, are also feasible.

ASSOCIATED CONTENT

Supporting Information

Details of monolayers grafting, monolayers' homogeneity characterization, supplementary spectroscopic measurements and evolution of energy levels. This information is available free of charge via the Internet at http://pubs.acs.org.

AUTHOR INFORMATION

Corresponding Author

*E-mail: David.Cahen@weizmann.ac.il.

Author Contributions

[§]Authors L.B.-N. and P.K.N. contributed equally to this work.

Notes

The authors declare no competing financial interest.

ACKNOWLEDGMENTS

We are grateful to the Israel Ministry of Science and Technology, the Wolfson Family trust, the Leona M. and Harry B. Helmsley Charitable Trust, the US-Israel Binational Science Foundation, the Israel Ministry of Science's "Tashtyoth" program and the Nancy and Stephen Grand Center for Sensors and Security for partial support. The authors thank I.D. Sharp for his guidance on SiC processing, and W. Li for the AFM topographic measurements. DC holds the Sylvia and Rowland Schaefer Chair in Energy research.

ABBREVIATIONS

Φ surface work function
A (electron) acceptor
AFM atomic force microscope
APTMS aminopropyltrimethoxy silane
CPD contact potential difference
D (electron) donor
FPTMS 3,3,3 (trifluoropropyl)trimethoxysilane
HOMO highest occupied molecular orbital
HTMS hexyltriemethoxy silane
KPFM Kelvin Probe Force Microscope
LUMO lowest unoccupied molecular orbital
MM molecular monolayers
OCS organic semiconducting materials
OTMS octyltrimethoxysilane
SWCA static water contact angle
UPS ultraviolet photoemission spectroscopy
V_{oc} open-circuit-voltage

REFERENCES

(1) Nayak, P. K.; Periasamy, N. Calculation of Electron Affinity, Ionization Potential, Transport Gap, Optical Band Gap and Exciton Binding Energy of Organic Solids Using "solvation" Model and DFT. *Org. Electron.* **2009**, *10*, 1396−1400.

(2) Piliego, C.; Loi, M. A. Charge Transfer State in Highly Efficient Polymer−Fullerene Bulk Heterojunction Solar Cells. *J. Mater. Chem.* **2012**, *22*, 4141−4150.

(3) Street, R. A.; Krakaris, A.; Cowan, S. R. Recombination Through Different Types of Localized States in Organic Solar Cells. *Adv. Funct. Mater.* **2012**, *22*, 4608−4619.

(4) Vandewal, K.; Tvingstedt, K.; Gadisa, A.; Inganäs, O.; Manca, J. V. Relating the Open-Circuit Voltage to Interface Molecular Properties of Donor:acceptor Bulk Heterojunction Solar Cells. *Phys. Rev. B* **2010**, *81*, 125204.

(5) Graham, K. R.; Erwin, P.; Nordlund, D.; Vandewal, K.; Li, R.; Ngongang Ndjawa, G. O.; Hoke, E. T.; Salleo, A.; Thompson, M. E.; McGehee, M. D.; Amassian, A. Re-evaluating the Role of Sterics and Electronic Coupling in Determining the Open-Circuit Voltage of Organic Solar Cells. *Adv. Mater.* **2013**, *25*, 6076−6082.

(6) Brabec, C. J.; Cravino, A.; Meissner, D.; Sariciftci, N. S.; Fromherz, T.; Rispens, M. T.; Sanchez, L.; Hummelen, J. C. Origin of the Open Circuit Voltage of Plastic Solar Cells. *Adv. Funct. Mater.* **2001**, *11*, 374−380.

(7) Scharber, M. C.; Mühlbacher, D.; Koppe, M.; Denk, P.; Waldauf, C.; Heeger, A. J.; Brabec, C. J. Design Rules for Donors in Bulk-Heterojunction Solar Cells-Towards 10% Energy-Conversion Efficiency. *Adv. Mater.* **2006**, *18*, 789−794.

(8) Gadisa, A.; Svensson, M.; Andersson, M. R.; Inganäs, O. Correlation between Oxidation Potential and Open-Circuit Voltage of Composite Solar Cells Based on Blends of Polythiophenes/Fullerene Derivative. *Appl. Phys. Lett.* **2004**, *84*, 1609−1611.

(9) Yamamoto, S.; Orimo, A.; Ohkita, H.; Benten, H.; Ito, S. Molecular Understanding of the Open-Circuit Voltage of Polymer:-Fullerene Solar Cells. *Adv. Energy Mater.* **2012**, *2*, 229−237.

(10) Kooistra, F. B.; Knol, J.; Kastenberg, F.; Popescu, L. M.; Verhees, W. J. H.; Kroon, J. M.; Hummelen, J. C. Increasing the Open Circuit Voltage of Bulk-Heterojunction Solar Cells by Raising the LUMO Level of the Acceptor. *Org. Lett.* **2007**, *9*, 551−554.

(11) Wilke, A.; Endres, J.; Hörmann, U.; Niederhausen, J.; Schlesinger, R.; Frisch, J.; Amsalem, P.; Wagner, J.; Gruber, M.; Opitz, A.; Vollmer, A.; Brütting, W.; Kahn, A.; Koch, N. Correlation between Interface Energetics and Open Circuit Voltage in Organic Photovoltaic Cells. *Appl. Phys. Lett.* **2012**, *101*, 233301.

(12) Rand, B. P.; Burk, D. P.; Forrest, S. R. Offset Energies at Organic Semiconductor Heterojunctions and Their Influence on the Open-Circuit Voltage of Thin-Film Solar Cells. *Phys. Rev. B* **2007**, *75*, 115327.

(13) Tada, A.; Geng, Y.; Wei, Q.; Hashimoto, K.; Tajima, K. Tailoring Organic Heterojunction Interfaces in Bilayer Polymer Photovoltaic Devices. *Nat. Mater.* **2011**, *10*, 450−455.

(14) Alloway, D. M.; Hofmann, M.; Smith, D. L.; Gruhn, N. E.; Graham, A. L.; Colorado, R.; Wysocki, V. H.; Lee, T. R.; Lee, P. A.; Armstrong, N. R. Interface Dipoles Arising from Self-Assembled Monolayers on Gold: UV−Photoemission Studies of Alkanethiols and Partially Fluorinated Alkanethiols. *J. Phys. Chem. B* **2003**, *107*, 11690−11699.

(15) Goh, C.; Scully, S. R.; McGehee, M. D. Effects of Molecular Interface Modification in Hybrid Organic-Inorganic Photovoltaic Cells. *J. Appl. Phys.* **2007**, *101*, 114503−114512.

(16) Liu, Y.; Scully, S. R.; McGehee, M. D.; Liu, J.; Luscombe, C. K.; Fréchet, J. M. J.; Shaheen, S. E.; Ginley, D. S. Dependence of Band Offset and Open-Circuit Voltage on the Interfacial Interaction between TiO_2 and Carboxylated Polythiophenes. *J. Phys. Chem. B* **2006**, *110*, 3257−3261.

(17) Vaynzof, Y.; Kabra, D.; Zhao, L.; Ho, P. K. H.; Wee, A. T.-S.; Friend, R. H. Improved Photoinduced Charge Carriers Separation in Organic-Inorganic Hybrid Photovoltaic Devices. *Appl. Phys. Lett.* **2010**, *97*, 033309.

(18) Kim, D. H.; Lee, H. S.; Yang, H.; Yang, L.; Cho, K. Tunable Crystal Nanostructures of Pentacene Thin Films on Gate Dielectrics Possessing Surface-Order Control. *Adv. Funct. Mater.* **2008**, *18*, 1363−1370.

(19) Shtein, M.; Mapel, J.; Benziger, J. B.; Forrest, S. R. Effects of Film Morphology and Gate Dielectric Surface Preparation on the Electrical Characteristics of Organic-Vapor-Phase-Deposited Pentacene Thin-Film Transistors. *Appl. Phys. Lett.* **2002**, *81*, 268−270.

(20) Forrest, S. R.; Burrows, P. E.; Haskal, E. I.; So, F. F. Ultrahigh-Vacuum Quasiepitaxial Growth of Model van Der Waals Thin Films. II. Experiment. *Phys. Rev. B* **1994**, *49*, 11309−11321.

(21) Bao, Z.; Lovinger, A. J.; Dodabalapur, A. Organic Field #x2010;effect Transistors with High Mobility Based on Copper Phthalocyanine. *Appl. Phys. Lett.* **1996**, *69*, 3066−3068.

(22) Duhm, S.; Hosoumi, S.; Salzmann, I.; Gerlach, A.; Oehzelt, M.; Wedl, B.; Lee, T.-L.; Schreiber, F.; Koch, N.; Ueno, N.; Kera, S. *Phys. Rev. B* **2010**, *81*.

(23) Fukagawa, H.; Yamane, H.; Kataoka, T.; Kera, S.; Nakamura, M.; Kudo, K.; Ueno, N. Origin of the Highest Occupied Band Position in Pentacene Films from Ultraviolet Photoelectron Spectroscopy: Hole Stabilization versus Band Dispersion. *Phys. Rev. B* **2006**, *73*, 245310.

(24) Liu, X.; Grueneis, A.; Haberer, D.; Fedorov, A.; Vilkov, O.; Strupinski, W.; Pichler, T. Tunable Interface Properties between Pentacene and Graphene on SiC Substrate. *J. Phys. Chem. C* **2013**, *117*, 3969−3975.

(25) Kim, J. S.; Park, J. H.; Lee, J. H.; Jo, J.; Kim, D.-Y.; Cho, K. Control of the Electrode Work Function and Active Layer Morphology via Surface Modification of Indium Tin Oxide for High Efficiency Organic Photovoltaics. *Appl. Phys. Lett.* **2007**, *91*, 112111.
(26) Bulliard, X.; Ihn, S.-G.; Yun, S.; Kim, Y.; Choi, D.; Choi, J.-Y.; Kim, M.; Sim, M.; Park, J.-H.; Choi, W.; Cho, K. Enhanced Performance in Polymer Solar Cells by Surface Energy Control. *Adv. Funct. Mater.* **2010**, *20*, 4381−4387.
(27) Opitz, A.; Wagner, J.; Brütting, W.; Salzmann, I.; Koch, N.; Manara, J.; Pflaum, J.; Hinderhofer, A.; Schreiber, F. Charge Separation at Molecular Donor−Acceptor Interfaces: Correlation Between Morphology and Solar Cell Performance. *IEEE J. Sel. Top. Quantum Electron.* **2010**, *16*, 1707−1717.
(28) Nayak, P. K.; Barnea-Nehoshtan, L.; Kim, R. S.; Shu, A.; Man, G.; Kahn, A.; Lederman, D.; Feldman, Y.; Cahen, D. The Effect of Structural Order on Solar Cell Parameters, as Illustrated in a SiC-Organic Junction Model. *Energy Environ. Sci.* **2013**, *6*, 3272−3279.
(29) Pernstich, K. P.; Haas, S.; Oberhoff, D.; Goldmann, C.; Gundlach, D. J.; Batlogg, B.; Rashid, A. N.; Schitter, G. Threshold Voltage Shift in Organic Field Effect Transistors by Dipole Monolayers on the Gate Insulator. *J. Appl. Phys.* **2004**, *96*, 6431−6438.
(30) Ulman, A. Formation and Structure of Self-Assembled Monolayers. *Chem. Rev.* **1996**, *96*, 1533−1554.
(31) Allara, D. L.; Parikh, A. N.; Rondelez, F. Evidence for a Unique Chain Organization in Long Chain Silane Monolayers Deposited on Two Widely Different Solid Substrates. *Langmuir* **1995**, *11*, 2357−2360.
(32) Schoell, S. J.; Hoeb, M.; Sharp, I. D.; Steins, W.; Eickhoff, M.; Stutzmann, M.; Brandt, M. S. Functionalization of 6H-SiC Surfaces with Organosilanes. *Appl. Phys. Lett.* **2008**, *92*, 153301.
(33) We Define a Surface Dipole as Negative (positive) If the Negative (positive) Pole Points Away from (towards) the Surface.
(34) Amassian, A.; Pozdin, V. A.; Desai, T. V.; Hong, S.; Woll, A. R.; Ferguson, J. D.; Brock, J. D.; Malliaras, G. G.; Engstrom, J. R. Post-Deposition Reorganization of Pentacene Films Deposited on Low-Energy Surfaces. *J. Mater. Chem.* **2009**, *19*, 5580−5592.
(35) Käfer, D.; Wöll, C.; Witte, G. Thermally Activated Dewetting of Organic Thin Films: The Case of Pentacene on SiO2 and Gold. *Appl. Phys. A: Mater. Sci. Process.* **2008**, *95*, 273−284.
(36) Ando, M.; Kawasaki, M.; Imazeki, S.; Sasaki, H.; Kamata, T. Self-Aligned Self-Assembly Process for Fabricating Organic Thin-Film Transistors. *Appl. Phys. Lett.* **2004**, *85*, 1849−1851.
(37) Nickel, B.; Barabash, R.; Ruiz, R.; Koch, N.; Kahn, A.; Feldman, L.; Haglund, R.; Scoles, G. Dislocation Arrangements in Pentacene Thin Films. *Phys. Rev. B* **2004**, *70*, 125401.
(38) Seo, H.-S.; Jang, Y.-S.; Zhang, Y.; Syed Abthagir, P.; Choi, J.-H. Fabrication and Characterization of Pentacene-Based Transistors with a Room-Temperature Mobility of 1.25°cm^2/Vs. *Org. Electron.* **2008**, *9*, 432−438.
(39) Deman, A.-L.; Erouel, M.; Lallemand, D.; Phaner-Goutorbe, M.; Lang, P.; Tardy, J. Growth Related Properties of Pentacene Thin Film Transistors with Different Gate Dielectrics. *J. Non-Cryst. Solids* **2008**, *354*, 1598−1607.
(40) Tsiper, E. V.; Soos, Z. G. Electronic Polarization in Pentacene Crystals and Thin Films. *Phys. Rev. B* **2003**, *68*, 085301.
(41) Topham, B. J.; Soos, Z. G. Ionization in Organic Thin Films: Electrostatic Potential, Electronic Polarization, and Dopants in Pentacene Films. *Phys. Rev. B* **2011**, *84*, 165405.
(42) Lee, Y. M.; Kim, J. W.; Min, H.; Lee, T. G.; Park, Y. Growth Morphology and Energy Level Alignment of Pentacene Films on SiO2 Surface Treated with Self-Assembled Monolayer. *Curr. Appl. Phys.* **2011**, *11*, 1168−1172.
(43) Chou, C.-T.; Lin, C.-H.; Tai, Y.; Liu, C.-H. J.; Chen, L.-C.; Chen, K.-H. Stacking Orientation Mediation of Pentacene and Derivatives for High Open-Circuit Voltage Organic Solar Cells. *J. Phys. Chem. Lett.* **2012**, *3*, 1079−1083.
(44) Natan, A.; Zidon, Y.; Shapira, Y.; Kronik, L. Cooperative Effects and Dipole Formation at Semiconductor and Self-Assembled-Monolayer Interfaces. *Phys. Rev. B* **2006**, *73*, 193310.
(45) Rissner, F.; Egger, D. A.; Romaner, L.; Heimel, G.; Zojer, E. The Electronic Structure of Mixed Self-Assembled Monolayers. *ACS Nano* **2010**, *4*, 6735−6746.
(46) Wu, K.-Y.; Yu, S.-Y.; Tao, Y.-T. Continuous Modulation of Electrode Work Function with Mixed Self-Assembled Monolayers and Its Effect in Charge Injection. *Langmuir* **2009**, *25*, 6232−6238.
(47) Petoral, R. M.; Yazdi, G. R.; Lloyd Spetz, A.; Yakimova, R.; Uvdal, K. Organosilane-Functionalized Wide Band Gap Semiconductor Surfaces. *Appl. Phys. Lett.* **2007**, *90*, 223904.
(48) Baur, B.; Steinhoff, G.; Hernando, J.; Purrucker, O.; Tanaka, M.; Nickel, B.; Stutzmann, M.; Eickhoff, M. Chemical Functionalization of GaN and AlN Surfaces. *Appl. Phys. Lett.* **2005**, *87*, 263901.